Heritage Science

RESEARCH

Open Access

In-situ non destructive investigation of contemporary outdoor bronze sculptures

Heehong Kwon[1] and Namchul Cho[2*]

Abstract

Indoor investigations are commonly used to assess the causes and extent of damage to bronze artwork and cultural heritage items; however, these methods typically involve destructive sampling and outdoor bronze sculptures are typically heavy and large, hindering their transport. In this study, 16 contemporary bronze sculptures exposed to outdoor environments for a period exceeding 20 years were evaluated in-situ to develop a non-destructive prediction model that can identify types of corrosion and quantify the amount of corrosion on bronze sculptures that cannot be easily transported. The sculptures were classified into three groups according to their patina chromaticity, reflectivity, and chemical composition. The corrosion characteristics were found to be copper oxide and sulfide patinas. Chromaticity and reflectivity investigations revealed that the chemical composition changes of the patinas corresponded to the formation of corrosion products, thus showing a high potential for the identification of the type of corrosion. Portable XRF spectroscopy showed that the low error rate of Cu make its compositional behavior a good indicator in identifying the type of corrosion of sulfide and chloride patinas. Portable Raman spectroscopy was able to detect basic sulfides such as brochantite, antlerite, and cuprite. The corrosion types and corrosion products on the bronze sculptures could be identified using chromaticity and reflectivity, portable X-ray fluorescence, and portable Raman spectroscopy. The rapid insitu diagnosis of these corrosion attributes is expected to contribute to establishing conservation treatment plans in the future.

Keywords In-situ investigation, Non-destructive investigation, Outdoor corrosion, Patina, Portable Raman spectroscopy, Portable XRF, Spectrum colorimeter

Introduction

One of the most common and effective methods for assessing the condition and safety of metal items of cultural heritage significance and artwork involves the investigation of production techniques, welding lines, casting defects, and previous repairs via visual observation, photography, optical examinations such as microscopy, as well as X-rays and gamma rays. In addition, to verify the types of metal damage and their causes, various scientific analysis methods are employed to identify corrosion byproducts.

Analytical methods such as X-ray diffraction (XRD), micro-Raman spectroscopy, and scanning electron microscopy with energy dispersive X-ray spectroscopy (SEM–EDS) are commonly used in indoor investigations to assess the causes and extent of damage to bronze; these methods typically involve destructive sampling. However, the scientific analysis and diagnosis of damage and surface corrosion products in indoor environments poses significant practical challenges. Furthermore, outdoor bronze sculptures are typically heavy and large, making them difficult to move. The limited sampling of artwork and cultural heritage items necessitate the application of non-destructive and non-invasive analytical methods

*Correspondence:
Namchul Cho
nam1611@kongju.ac.kr
[1] Department of Conservation and Art Bank, National Museum of Modern and Contemporary Art, Cheong Ju 28501, Republic of Korea
[2] Department of Cultural Heritage Conservation Science, Kongju National University, Gongju 32588, Republic of Korea

that can be measured in outdoor environments. Because sampling is conducted in small quantities, results are limited to a partial understanding and interpretation of the analysis target, with further disadvantages of analysis time and cost.

Non-destructive analysis methods such as chromaticity and portable X-ray fluorescence (XRF) analysis have been utilized in the preservation of cultural heritage pieces and artwork owing to their rapid and easy measurement, as well as the ability to compare and analyze statistical data. Characterizing and analyzing the unique color and alloy composition of metal artifacts based on the type of bronze corrosion products could provide valuable information in the form of primary on-site data without requiring specimen sampling or moving of the target artwork. Chromaticity analysis has utilized in research on the color change and characterization of patinas [1–10]. Portable XRF has been utilized for the identification and quantification of bronze patinas and layers [11–16]. Research on corrosion products, previously centered around indoor laboratories, has since been applied to situ investigations using portable Raman spectroscopy [16–24].

Many studies have reported that sulfide and chloride are among the most common and important corrosive byproducts [5, 25–33]. Chloride patina can lead to pitting and bronze disease, making its early identification crucial [34]. In our previous studies, we conducted artificial patina corrosion experiments to identify various types of corrosion and their correlation among outdoor bronze sculptures and to obtain standard data on sulfide and chloride patinas, which are major air pollutants in urban-industrial and marine environments [34, 35].

This study aimed to develop a prediction model that can identify the type of corrosion and quantify the amount of corrosion on large, heavy bronze sculptures in outdoor environments using non-destructive analysis methods. The objective of the study was to quickly diagnose the corrosion type and preservation status of outdoor bronze sculptures, providing initial data for establishing preservation plans. Using the analysis results obtained from artificial patina corrosion experiments [34, 35], we examined the corrosion type and applicability of the patinas of 16 bronze sculptures exposed to outdoor environments for over 20 years. Specifically, data obtained from spectrocolorimeters, portable XRF, and portable Raman spectrometers, commonly used in the preservation of metal cultural heritage items and artwork, were compared and analyzed.

Research method

Research elements

We selected 16 bronze sculptures made from quaternary bronze (Cu–Zn-Sn–Pb) alloys from the National Museum of Modern and Contemporary Art (MMCA) collection. These sculptures were chosen as their small differences in alloy compositions and have been exposed to outdoor environments for an extended period of time (Table 1). Previous research on bronze corrosion mechanisms focused on binary (Cu-Sn) and ternary (Cu-Sn–Pb)

Table 1 Bronze sculptures from the MMCA collection exposed to outdoor environments for over 20 years

No	Artist	Artwork	Production year	Composition (wt%)				
				Cu	Zn	Sn	Pb	Total
SC1	Changjo Han	Gate of history	1979	89.31	4.05	3.61	3.03	100
SC2	Sangkap Lee	Between 80	1980	85.05	3.01	6.16	5.78	100
SC3	Jeongsoo Koh	Sisters II	1981	87.20	5.73	2.89	4.18	100
SC4	Seunghwan Cho	You-83-arirang	1983	86.87	5.89	3.29	3.95	100
SC5	Dalsul Kwon	Visual point-opener	1984	84.3	6.9	5.3	3.5	100
SC6	Changhee Kim	Melody	1984	92.14	2.88	2.14	2.84	100
SC7	Hyosook Kim	Circle	1986	92.13	4.23	2.54	1.10	100
SC8	Kiok Park	Weaving	1986	87.57	5.63	2.50	4.30	100
SC9	Joon Chon	Voice-at the stone wall	1986	86.65	5.94	2.61	4.80	100
SC10	Manlin Choi	Womb, work 86–5-2	1986	89.36	5.71	2.78	2.15	100
SC11	Yoonhwa Kim	Eternal revolution-90	1990	87.60	5.25	3.12	4.03	100
SC12	Jungsoo Shim	West coast-conch	1994	85.58	5.89	4.02	4.51	100
SC13	Youngsun Lim	Family statue-outing	1996	88.19	6.60	2.00	3.21	100
SC14	Hyunsoo Hwang	Competing life	1996	86.58	5.66	3.92	3.84	100
SC15	Hoyong Kim	Object-self	1997	86.71	5.99	3.94	3.36	100
SC16	Mansul Kim	History I	1999	88.68	6.62	2.03	2.67	100

bronzes. However, the more than 500 bronze sculptures produced in Korea and other countries since the twentieth century are predominantly made from quaternary alloys (Cu–Zn-Sn–Pb) [36–42].

Analysis method

Microscopic observation

Portable microscopy (DG-3, Scalar, JP) and digital microscopy (RH-2000, Hirox, JP) were used to observe the surface morphology and condition of the outdoor bronze sculptures and artificial patinas.

Chromaticity and reflectivity analysis

Chromaticity and reflectivity analyses were conducted using a spectrocolorimeter (CR-400, Minolta, JP) in specular component excluded mode with a measurement diameter of 3 mm. The surface reflectivity was calculated as the average of five measurements taken in the visible light range of 350–750 nm. Chromaticity and reflectivity were measured at 2–4 points on the bronze sculptures by selecting areas with colors different from the base metal.

Portable XRF analysis

Non-destructive chemical composition analyses were conducted using a portable XRF spectrometer (Alloy Plus, Olympus Delta, USA). The analysis was conducted under the following conditions: The collimator of the detector is 15 mm in diameter and Resolution ranges from 145 to 316 eV. 40 kV with Alumina filter for 10 s, and 8 kV without a filter for 30 s. The concentrations (ppm, wt%) of the main constituent elements of bronze, Cu, Zn, Sn, and Pb were determined and converted into percentages for the four elements.

Portable Raman spectroscopy

The Raman spectra were acquired using a portable Raman spectrometer (I-Raman Prime, B&W Tek, USA). 6mW diode laser at a wavelength of 532 nm was applied as an excitation source, and the output power of the laser at the exiting probe was 35mW, nominal. The spectral range was between 150 to 4200 Cm^{-1}, with a resolution of 7.3 cm^{-1}.

Atmospheric environment of bronze sculptures

Air pollutant concentration and rainwater acidity are factors that influence the corrosion of outdoor bronze sculptures. Thus, air pollution levels (1990–2022) and major ion concentrations of acid depositions (1999–2022) at the MMCA in Gwacheon, Gyeonggi-do, South Korea are shown in Fig. 1 [43]. This could indicate the correlation between the corrosion of outdoor bronze sculptures and atmospheric pollutants.

Regarding the air pollution status, SO_2 levels have shown a consistent decreasing trend since 1990 with some levels exceeding the standard of 0.02 ppm in the early 1990s. However, the steady decline reached 0.003 ppm in 2022. Although NO_2 levels have fluctuated around the standard value of 0.03 ppm, a decreasing trend has been observed since 2016. Over the past 30 years, O_3 has consistently remained within the standard value of 0.06 ppm; however, an overall increasing trend has been observed. CO has exhibited a general decreasing trend within the standard range.

Regarding the major ionic concentrations in annual acid depositions, anions such as SO_4^{2-}, NO_{3-}, and Cl^- become strongly acidic when combined with hydrogen ions. These ion concentrations have shown a continuous increasing trend since 1999 when measurements were first taken but started to decrease overall in the early to mid-2010s. Furthermore, the average pH of rainwater measured from 1990 to 2022 in Seoul, located approximately 10 km from Gwacheon, Gyeonggi-do, was 4.8, indicating acidification, with pH 5.6 representing neutrality [43, 44].

Results and discussion

Microscopic observation

The color of the patinas on the surfaces of the 16 bronze sculptures that had been exposed to outdoor environments for over 20 years were all shades of green and classified into three main groups (Fig. 2a).

The type I dark green patina layers (sculptures SC1, SC3, SC4, SC6, SC8, SC9, S11, SC12, SC14, SC15) were observed to have mostly flat and dense surfaces. The type II patina layers were light green (sculptures SC5, SC7, SC10, SC13, SC16), and the type III patina layer was close to a light blue patina (sculpture SC2). In general, patina formed in urban atmosphere is known to have less porosity and higher adhesion compared to marine patina [45], and differences in the condition of the surface were also confirmed depending on the color of the patina [34, 35].

A comparison between the surface conditions of the outdoor bronze sculptures' natural and artificial patinas revealed differences in density and other characteristics. The reason for these differences was determined to be the weak adhesion and porosity between the base layer and artificial patina generated over a short period of time. Furthermore, the outdoor bronze sculptures had been exposed to an acidic environment with an average pH of 4.8 and atmospheric pollutants such as SO_2 and NO_2 for over 20 years, as confirmed by the current levels of air pollution and acid depositions in the area. The corrosion type and patterns were anticipated to be similar owing to the similar alloy compositions and close proximity

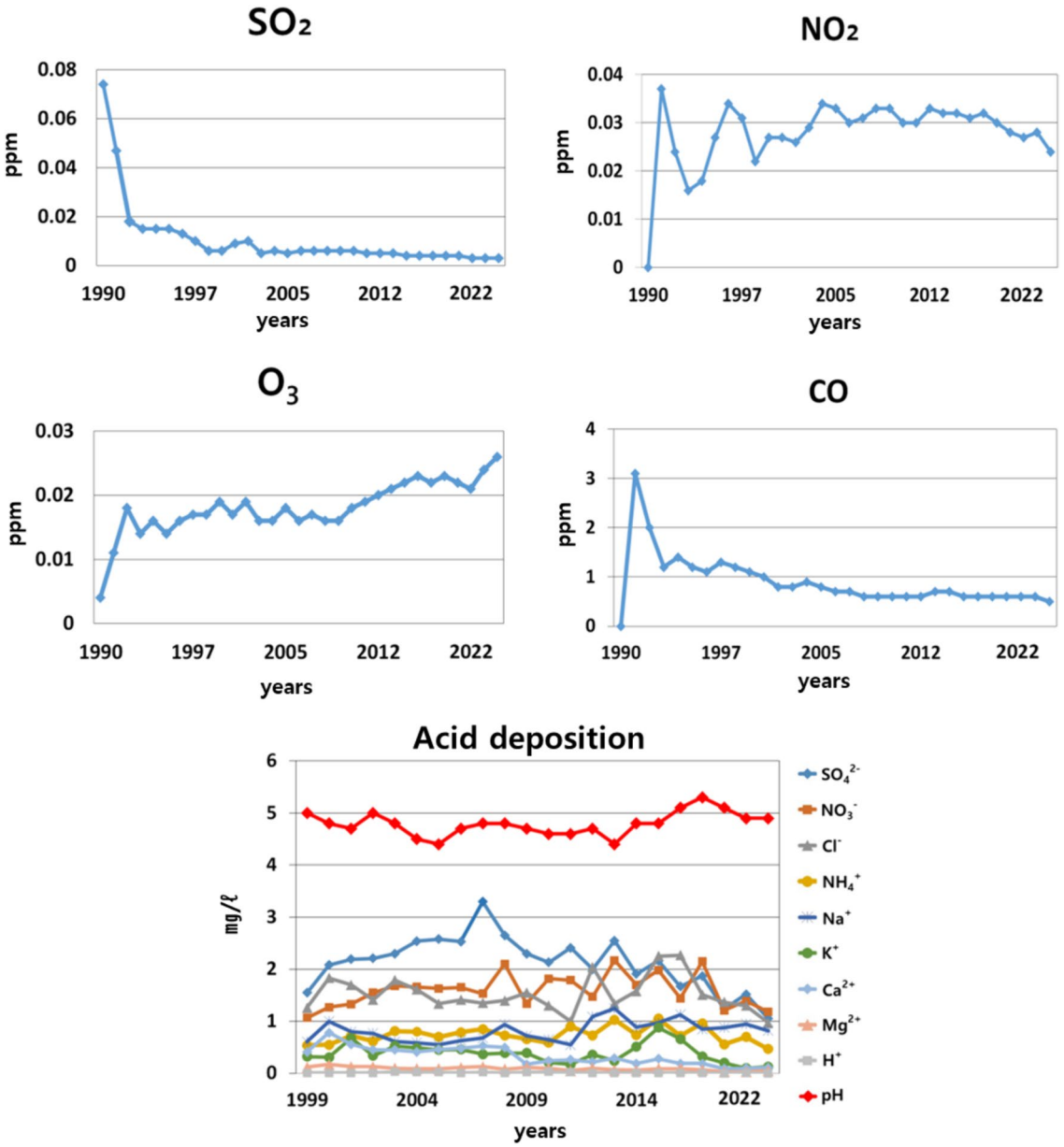

Fig. 1 Air pollution status and major ionic component concentrations of acid depositions of the environments surrounding the outdoor bronze sculptures: ppm (SO_2, NO_2, O3, and CO), and mg/l (acid deposition)

within a 300-m radius; however, differences in the color and surface conditions of the patinas were observed. This is likely owing to various parameters such as the surface condition at the time of production, solubility of the corrosion products, presence of protective measures (e.g., surrounding vegetation), different corrosion conditions (e.g., bird droppings, pollen, and pine pollen), preservation treatments (wax coating), and impurities within the alloy (segregation).

Chromaticity and reflectivity analysis

The chromaticity and reflectivity analyses revealed that the patinas on the surfaces of the 16 bronze sculptures were all in the green color range and could be classified into three main groups. The change in the b* value was relatively small compared to the significant changes observed in the L* and a* values. Based on the analyses of actual sculptures, the chromaticity and reflectivity as well as the applicability of sulfide and chloride artificial

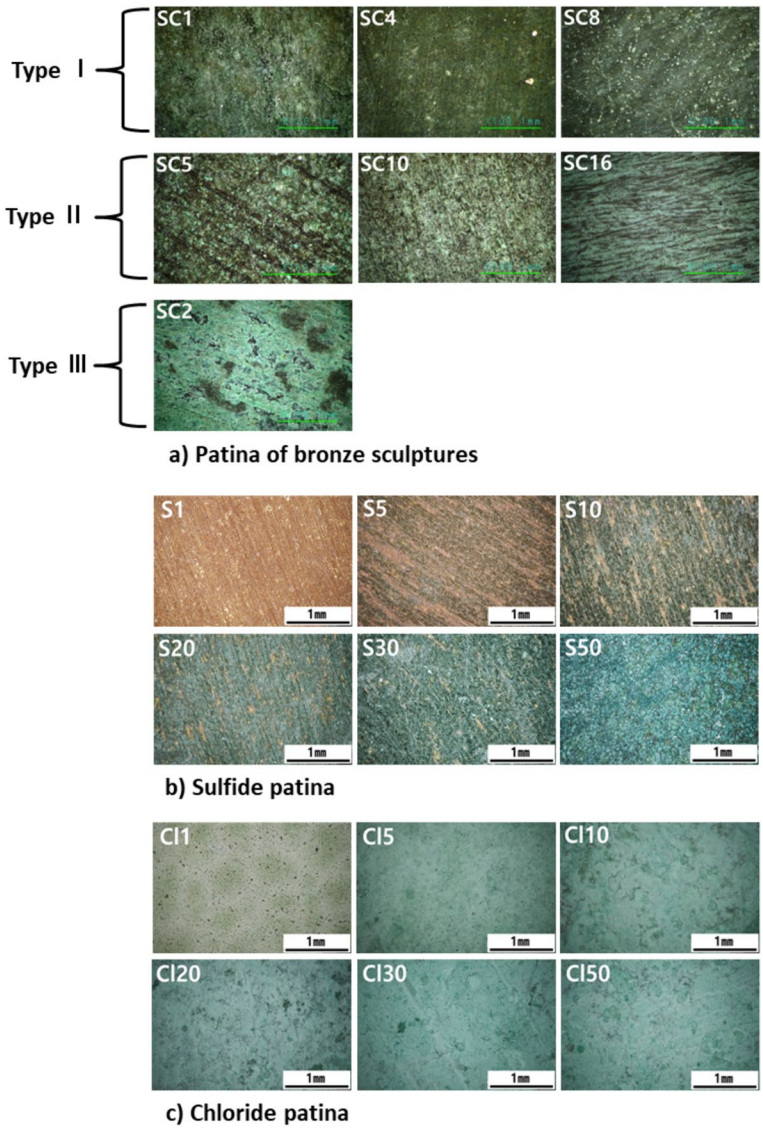

Fig. 2 Microscopic observations of outdoor bronze sculptures' patinas and artificial patinas: **a** patina of bronze sculptures, **b** sulfide patina, and **c** chloride patina

patinas were evaluated through artificial patina corrosion experiments (Figs. 3 and 4).

The sulfide artificial patina closely resembled the surface patina color of bronze sculptures exposed to outdoor corrosion (Fig. 3). The L* value gradually increased from 53.50 to 58.86, indicating a brightening effect. The analysis of the b* values representing the yellow–blue color showed no significant changes after the initial stage (S5), but gradually shifted toward the blue color. Specifically, the analysis of the a* values representing the red–green color revealed a color shift similar to that of outdoor bronze sculptures (-8 to 0), and the L* values were also within the brightness range of the bronze sculptures. The correlation between the growth of patina and chromaticity of the outdoor bronze sculptures was confirmed to progress from type I to type II to type III by the chromaticity and corrosion behaviors of the artificial sulfide patina.

The chloride artificial patina showed a significant difference in L* values of 20–40 compared to the artwork, with a* and b* values concentrated in the ranges of -18 to -15 and -3.6 to 6.4, respectively, indicating differences from the actual patina colors of the sculptures.

The reflectivity analysis yielded similar results (Fig. 4). The reflectivity of the outdoor bronze sculpture revealed low reflectivity across all wavelength ranges, gradually

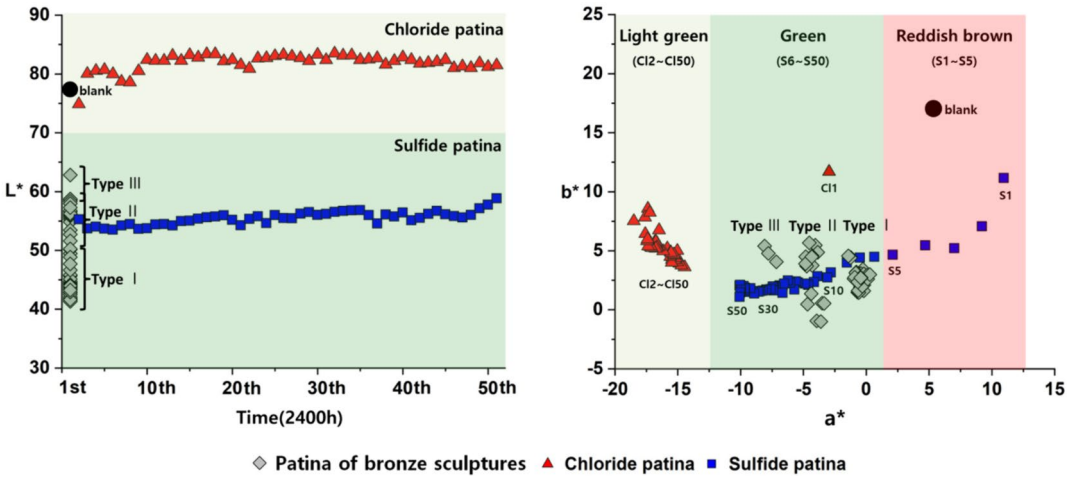

Fig. 3 Chromaticity comparison between outdoor bronze sculptures and artificial patinas: The chromaticity values of the bronze sculptures' patinas are in the chromaticity range of the sulfide patina

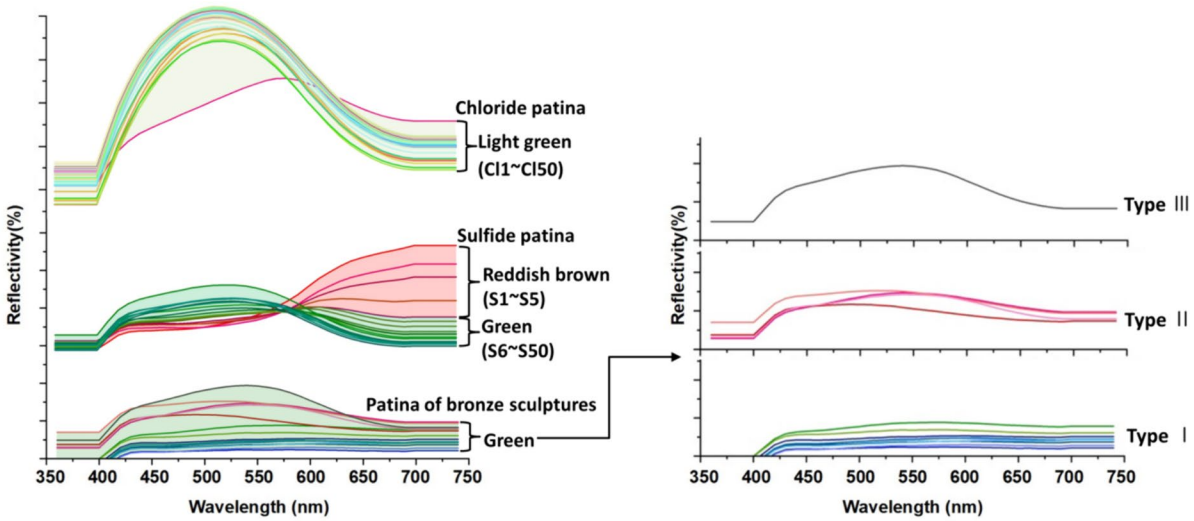

Fig. 4 Reflectivity comparison between outdoor bronze sculptures and artificial patinas: The reflectivity values of the bronze sculptures' patinas are in the reflectivity range of the sulfide patina (green)

increasing in the blue (380–500 nm) and green (500–565 nm) spectra. However, a decrease in reflectivity was observed as the transition was made from the yellow (565–625 nm) to the red (625–750 nm) spectrum. The patina of alkaline sulfide also exhibited a similar spectrum to that of the sculpture. The blue–green spectrum increased, whereas the yellow–red spectrum decreased consistent with the corrosive behavior. The artificial chloride patina exhibited higher reflectivity than the artificial sulfide patina in all wavelength ranges for the outdoor bronze sculptures. Particularly, a reflectivity difference of 40–50% or higher was observed in the blue–green spectrum.

The above findings confirm the possibility of identifying corrosion type for bronze sculptures using the chromaticity and reflectivity of artificial patinas. Chromaticity was found to be particularly suitable for the quantitative comparison with other colors, while reflectivity was useful for identifying the corrosion type of specific colors. However, the wide distribution values of brightness and reflectivity of outdoor bronze sculptures also showed discrepancies (L^* was approximately 12–17) for the artificial sulfide patina. The differences in surface conditions of natural and artificial patinas on outdoor bronze sculptures are influenced by factors such as dust, pollen, and atmospheric pollutants, which affect the

brightness and reflectivity of the sculptures. In addition, the optical characteristics of the patina surface can be altered by light diffraction and absorption, as well as interference effects such as the patina layer thickness, refractive index, and incident light.

One of the crucial factors in distinguishing bronze patinas is known to be the L^* value [10]. According to the optical properties of materials, an object's reflectivity generally influences its color and brightness. When an object exhibits higher reflectivity across all wavelengths compared to the reference, it appears brighter [46]. The artificial chloride patina exhibited a brightness (L^*) value more than 20 higher than that of the outdoor bronze sculpture and artificial sulfide patina, with high reflectivity observed across all wavelength ranges. In particular, a difference of 40–50% or higher in reflectance was observed in the blue–green spectrum. This suggests that brightness (L^*) can be used in conjunction with reflectivity to identify the type of corrosion of a bronze patina.

Portable XRF analysis

The chemical compositions of the patina surfaces of the 16 bronze sculptures were classified into three main groups. Based on the analysis of actual sculptures, the results of the corrosion experiment components of sulfide and chloride artificial patinas were compared, and the applicability was assessed using a Zn-Sn–Pb ternary diagram (Fig. 5).

The artificial sulfide patina exhibited a tendency similar to the alloy composition of bronze sculpture type I. When compared and analyzed based on bronze sculpture type I, the standard deviations of the elements were found to be 2 wt% for Cu, -1 wt% for Zn, -0.5 wt% for Sn, and -0.5 wt% for Pb. We attempted to observe changes in the alloy elements resulting from artificial patina corrosion behavior in a ternary system; however, no significant changes were observed in the ternary diagram. This suggests that significant compositional changes are unlikely in a short period of time (2400 h).

The chemical compositions of artificial chloride patinas were broadly classified into three groups: type A (Cl1–Cl3) for early corrosion, type B (Cl4–Cl25) for intermediate corrosion, and type C (Cl26–Cl50) where Zn was not detected. Specifically, type A was distributed along the boundary of the bronze sculptures type I and type II, whereas the other groups exhibited differed significantly from the sculpture composition.

The chemical composition of the outdoor bronze sculptures showed an overall decrease in Cu and Zn contents, whereas the Sn content exhibited an increasing trend. However, a consistent trend was difficult to demonstrate owing to factors such as alloy composition, corrosion degree, surface condition, and various environmental parameters. Furthermore, the XRF analysis from the surface, depending on the chemical element considered due to the Beer-Lambert law the measurement does not concern the same depth. In general, measurement of the elements Cu and Zn is done over a depth of approximately 200 to 300 μm while that of Sn and Pb is done over more than 1 mm [45]. However, in this study, we were not able to measure the thickness of the patina layer. Notwithstanding, Cu exhibited distinct differences in composition from the other elements

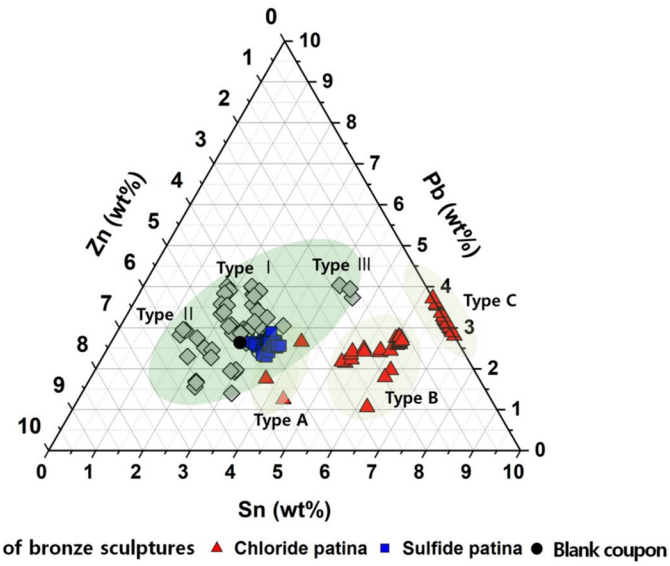

Fig. 5 Comparison of the chemical composition of outdoor bronze sculptures and artificial patinas

according to the corrosion behaviors of the sulfide patina (87.47 → 89.04 wt%) and chloride patina (88.8 → 78.2 wt%). Hence, the compositional differences according to the corrosion behavior of Cu are likely highly applicable in identifying the corrosion type of sulfide and chloride patinas.

The identification and quantification of patina layers are known to be achievable in the range of 20–100 μm using p-XRF, depending on factors such as the alloy of bronze and the degree of corrosion [11, 14]. In particular, owing to environmental influences, the patina layer on bronze artifacts exposed to outdoor conditions is expected to be thin and less complex in terms of corrosion mechanisms than artifacts with thick patina layers. Therefore, portable XRF analysis is expected to be applicable.

Portable Raman spectroscopy

Before analyzing the corrosion products on the patina surfaces of the outdoor bronze sculptures in the field, previous studies have already conducted preliminary analyses on the corrosion products of sulfide and chloride artificial patinas [34, 35]. The potential applicability of portable Raman spectroscopy was confirmed by comparing the analysis results of the corrosion products on the surfaces with artificial patinas using XRD, benchtop Raman microspectroscopy, and portable Raman spectroscopy.

An analysis of the portable Raman spectroscopy on the patina surfaces of the 16 outdoor bronze sculptures revealed the presence of cuprite, brochantite, and antlerite (Fig. 6). Raman shifts at 214, 216, and 218 cm^{-1} were detected in eight sculptures (SC1, SC4, SC7, SC8, SC10, SC12, SC13, SC14), closely matching those of cuprite (Cu_2O). The similarity in Raman shifts and peak shapes confirmed the presence of cuprite.

Raman shifts of 384, 480, and 973 cm^{-1} were detected in 12 sculptures (SC1, SC2, SC4, SC6, SC7, SC9, SC10, SC11, SC12, SC14, SC15, SC16). These were confirmed to be brochantite ($Cu_4SO_4(OH)_6$), as their Raman shift closely matched that of alkaline sulfide, and their peak shapes were also similar. In particular, cuprite and brochantite were detected together in 6 sculptures (SC1, SC4, SC7, SC10, SC12, SC14).

In two sculptures (SC11, SC15), Raman shifts of 420, 973, and 1047 cm^{-1} were detected, closely matching the Raman shift of the basic sulfide antlerite ($Cu_3SO_4(OH)_4$). The similarity in peak shape further confirmed the presence of antlerite. In particular, the characteristic peaks (971 and 973 cm^{-1}) of antlerite and broochantite are similar. Therefore, the two compounds were classified by Raman shift of 1044 and 1047 cm^{-1}.

Additional verification and research are deemed necessary for two sculptures, SC3 and SC5, owing to difficulty in accurately identifying the compounds present in these sculptures.

These results are consistent with previous visual and microscopic observations, chromaticity and reflectivity, and portable XRF analysis results. Thus, we confirmed that the identification of corrosion type and the corrosion products of a bronze sculpture is possible using portable Raman spectroscopy.

When bronze is exposed for decades to the outdoor environment contaminated with SO_2, the SO_2 dissolves in the surface moisture and reacts with the bronze to form alkaline sulfides. The most commonly observed alkaline sulfide in outdoor bronze sculptures is green brochantite. Brochantite is typically stable under acidic conditions (pH 3.5–6), while antlerite is commonly found in regions with low acidity (pH 3.5 or lower) and high concentrations of sulfates.

In actual outdoor environments, acidity from rain, snow, and fog can dissolve copper corrosion products on the outermost layer and promote the alteration of minerals. Two examples are brochantite and antlerite. When the acidity of the water membrane where corrosion occurs increases (pH 3.5 or lower), brochantite dissolves and antlerite is formed. However, the formation of antlerite requires the prolonged maintenance of acidic conditions in the water membrane layer over a significant period. A short duration of acidic conditions can prevent the growth of antlerite and allow the surface recrystallization of brochantite. Thus, antlerite has been reported to form first in the lower parts or relatively less exposed areas of outdoor bronze sculptures where the moisture evaporation rate is lower [25, 29, 47]. Therefore, the presence of antlerite indicates a higher level of contamination, requiring increased caution regarding potential damage.

Conclusion

This study aimed to develop a prediction model that can identify corrosion type and quantify the amount of corrosion on large, heavy bronze sculptures in outdoor environments using non-destructive analysis methods. The corrosion types and preservation status of outdoor bronze sculptures were quickly diagnosed to establish a preservation plan. We investigated the corrosion patterns of artificial patinas through experimentation and evaluated the identified corrosion types and applicability for 16 bronze sculptures exposed to outdoor environments for over 20 years. Specifically, data obtained from spectrocolorimeters, portable XRF, and portable Raman spectrometry, commonly used for the preservation of metal cultural heritage artifacts and artwork, were compared and analyzed. The results are summarized as follows.

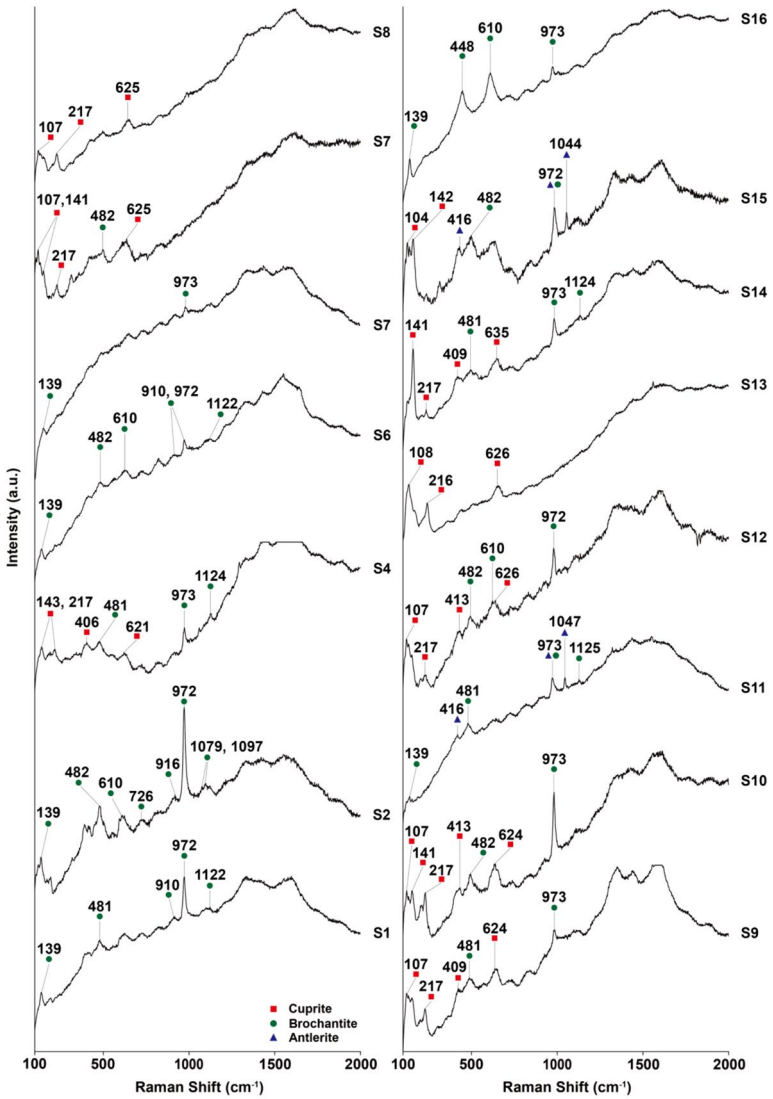

Fig. 6 Portable Raman spectroscopy graphs of outdoor bronze sculptures

The 16 bronze sculptures exposed to outdoor environments for over 20 years were classified into three groups based on patina chromaticity, reflectivity, and chemical composition. The corrosion characteristics were identified as copper oxide and sulfide patinas, such as cuprite, brochantite, and antlerite, commonly formed in urban-industrial atmospheric environments.

According to the evaluation of the chromaticity, reflectivity, and applicability of the outdoor bronze sculptures' patinas and artificial chloride patina, the colors of the bronze sculptures' patinas differed significantly. In contrast, the artificial sulfide patina was found to closely resemble the patina color of outdoor bronze sculptures owing to its corrosion behavior. Specifically, the a^* value representing red–green showed a similar color variation to that of outdoor bronze sculptures, and the L^* value also fell within the brightness range of bronze sculpture. Furthermore, the density of the patina surface decreased, while its porosity increased according to the corrosive behavior. We also confirmed the relationship between the patina growth on outdoor bronze sculptures and its chromaticity. Specifically, a turning point existed where 20% of the reflectivity in the yellow–red (565–750 nm) range could identify cuprite and brochantite. Furthermore, the chromaticity L^* value was found to be an important factor in identifying corrosion type along with reflectivity. Some discrepancies in brightness and

reflectivity values were observed depending on the surface condition and level of contamination of the patina. However, the chemical composition changes of the patina corresponded to the formation of corrosion products, indicating a high potential for identifying corrosion type.

The result of using portable XRF spectroscopy to assess the applicability of chemical composition revealed that, some of the bronze sculptures (Type I) showed a similar tendency in alloy composition to sulfide artificial patina. However, no significant changes were observed in the ternary diagram. This suggests that significant compositional changes are unlikely in a short period of time (2400 h). In addition, a consistent trend was difficult to demonstrate owing to factors such as alloy composition, corrosion degree, surface condition, and various environmental parameters. Nevertheless, the element Cu exhibited lower error rates than other elements, indicating that differences in composition owing to the corrosion behavior of Cu could be highly applicable in identifying the type of corrosion of sulfide and chloride patinas.

Upon evaluating the on-site applicability of portable Raman spectroscopy, basic sulfides such as brochantite, antlerite, and cuprite were detected. The XRD and bench-top Raman spectroscopy results of the previous artificial patina corrosion experiments confirmed the presence of brochantite and cuprite in the sulfide artificial patina, indicating a high potential for the application of portable Raman spectroscopy.

This study confirmed the feasibility of using portable non-destructive analytical equipment in outdoor environments to identify corrosion types and quantify corrosion amounts for large, heavy bronze sculptures. The findings of this study can provide important information as primary data in outdoor locations and are expected to be utilized for promptly diagnosing the types of corrosion affecting bronze sculptures in outdoor environments and their conservation status to establish conservation treatment plans.

Abbreviations

XRD	X-ray diffraction
SEM–EDS	: Scanning electron microscopy with energy dispersive X-ray spectroscopy
XRF	: X-ray fluorescence
MMCA	: National Museum of Modern and Contemporary Art

Acknowledgements
Not applicable.

Author contributions
NC- conceptualization, resources, writing-review and editing, supervision, project Administration. HK- methodology, software, validation, data curation, writing-original draft preparation, visualization, funding acquisition. All authors have read and agreed to the published version of the manuscript.

Funding
This research was funded by the Conservation Science Research Project of the National Museum of Modern and Contemporary Art, Republic of Korea (MMCA).

Availability of data and materials
All data generated or analyzed during this study are included in this published article.

Declarations

Competing interests
The authors declare that they have no competing interests.

Received: 15 March 2024 Accepted: 17 May 2024
Published online: 28 May 2024

References

1. Franey JP, Davis ME. Metallographic studies of the copper patina formed in the atmosphere. Corros Sci. 1987;27:659–68.
2. Livingston RA. Influence of the environment on the patina of the Statue of Liberty. Environ Sci Tech. 1991;25:1400–8.
3. Morcillo M, Almeida E, Marrocos M, Rosales B. Atmospheric corrosion of copper in Ibero-America. Corrosion. 2001;57(11):967–80.
4. Franceschi E, Letardi P, Luciano G. Colour measurements on patinas and coating system for outdoor bronze monuments. J Cult Herit. 2006;7:166–70.
5. Fitzgerald KP, Nairn J, Skennerton GA, Atrens. Atmospheric corrosion of copper and the colour, structure and composition of natural patinas on copper. Corros Sci. 2006;48:2480–509.
6. Goidanich S, Toniolo L, Jafarzadeh S, Wallinder IO. Effects of wax-based anti-graffiti on copper patina composition and dissolution during four years of outdoor urban exposure. Herit Sci. 2010;11:288–96.
7. Goidanich S, Brunk J, Herting G, Arenas M, Wallinder IO. Atmospheric corrosion of brass in outdoor applications: patina evolution, metal release and aesthetic appearance at urban exposure conditions. Sci Total Environ. 2011;412–413:46–57.
8. Gianni L, Adriaens A, Cavallini M, Natali S, Volpe V, Zortea L. Reflectance curves and CIE L* a* b* parameters to describe patina characteristics and corrosion mechanism on bronze alloys. CCSJ. 2014;2:38–43.
9. Devogelaere J. The Colour Palette of Antique Bronzes: An Experimental Archaeology Project. EXARC. 2017. https://exarc.net/issue-2017-2/ea/colour-palette-antique-bronzes-experimental-archaeology-project.
10. Leygraf C, Chang T, Herting G, Wallinder IO. The origin and evolution of copper patina colour. Corros Sci. 2019;157:337–46.
11. Porcaro M, Depalmas A, Lins S, Bulla C, Pischedda M, Brunetti A. Nuragic working tools characterization with corrosion layer determinations. Mater. 2022;15(11):3879.
12. Šatović D, Desnica V, Fazinić S. Use of portable X-ray fluorescence instrument for bulk alloy analysis on low corroded indoor bronzes. Spectrochim Acta B. 2013;89:7–13.
13. Buccolieri G. X-ray fluorescence for the study of the patinas on an outdoor bronze monument. Int J Conserv Sci. 2016;7(4):1009–22.
14. Robotti S, Rizzi P, Soffritti C, Garagnani GL, Greco C, Facchetti F, et al. Reliability of portable X-ray Fluorescence for the chemical characterisation of ancient corroded copper tin alloys. Spectrochim Acta Part B. 2018;146:41–9.
15. Sebar LE, Iannucci L, Gori C, Re A, Parvis M, Angelini E, et al. In-situ multi-analytical study of ongoing corrosion processes on bronze artworks exposed outdoors. ACTA IMEKO. 2021;10(1):241–9.
16. Madariaga JM. Analytical chemistry in the field of cultural heritage. Anal Methods. 2015;7(12):4848–76.
17. Porcu D, Innocenti S, Galeotti M, Striova J, Dei L, Carretti E, et al. Spectroscopic and morphologic investigation of bronze disease: performance evaluation of portable devices. Heritage. 2022;5(4):3548–61.

18. Colomban P, Tournié A, Maucuer M, Meynard P. On-site Raman and XRF analysis of Japanese/Chinese bronze/brass—the search for specific Raman signatures. J Raman Spectrosc. 2011;43(6):799–808.
19. Aramendia J, Gomez-Nubla L, Castro K, Martinez-Arkarazo I, Vega D, Sanz López de Heredia A, et al. Portable Raman study on the conservation state of four CorTen steel-based sculptures by Eduardo Chillida impacted by urban atmospheres. J Raman Spectrosc. 2012;43(8):1111–7.
20. Jehlička J, Culha A. Critical evaluation of portable Raman spectrometers: from rock outcrops and planetary analogs to cultural heritage—a review. Anal Chim Acta. 2022;1209: 339027.
21. Rosaki A, Vandenabeele P. In situ Raman spectroscopy for cultural heritage studies. J Raman Spectrosc. 2021;52(12):1–12.
22. Madariaga JM. Analytical strategies for cultural heritage materials and their degradation: introduction to analytical strategies for cultural heritage. London: Royal Society of Chemistry; 2021. p. 3–21.
23. Edwards HGM. Spectroscopic properties of inorganic and organometallic compounds: Raman spectroscopy of inorganic materials in art and archaeology: spectroscopic analysis of historical mysteries. London: Royal society of chemistry; 2009. p. 16–48.
24. Edwards HGM, Vandenabeele P, Colomban P. Raman spectroscopy in cultural heritage preservation : In-field and on-site raman analysis. Berlin: Springer; 2022. p. 395–412.
25. Robbiola L, Fiaud C, Pennec S. New model of outdoor bronze corrosion and its implications for conservation. ICOM Committee for Conservation 10th triennial meeting. Washington; 1993. P. 796–801.
26. Strandberg H. Reactions of copper payina compounds—I. influence of some air pollutants. Atmos Environ. 1998;32(20):3511–20.
27. Krätschmer A, Wallinder IO, Leygraf C. The evolution of outdoor copper patina. Corros Sci. 2022;44:425–49.
28. Selwyn L. Metal and corrosion : a handbook for the conservation professional. Ottawa: Canadian conservation institute; 2004. p. 63–4.
29. Fuente D, Simancas J, Morcillo M. Morphological study of 16-year patinas formed on copper in a wide range of atmospheric exposures. Corros Sci. 2008;50:268–85.
30. Leygraf C, Wallinder IO, Tidblad J, Graedel T. Atmospheric corrosion. 2nd ed. Hoboken: Wiley; 2016. p. 292–9.
31. Catelli E, Sciutto G, Prati S, Jia Y, Mazzeo R. Characterization of outdoor bronze monument patinas: the potentialities of near-infrared spectroscopic analysis. ESPR. 2018;25:24379–93.
32. Zahner LW. Copper, brass, and bronze surfaces : a guide to alloys, finishes, fabrication, and maintenance in architecture and art. Hoboken: John Wiley & Sons Inc; 2020. p. 6-13, 105-113, 263-266, 295–296.
33. Apchain E, Neff D, Gallien JP, Nuns N, Berger P, Noumowe A, et al. Efficiency and durability of protective treatments on cultural heritage copper corrosion layers. Corros Sci. 2011;183:109319.
34. Kwon H. Corrosion behaviors of artificial chloride patina for studying bronze sculpture corrosion in marine environments. Coatings. 2023;13(9):1630.
35. Kwon H, Cho N. Corrosion behaviors of outdoor bronze sculptures in an urban–industrial environment: corrosion experiment on artificial sulfide patina. Metals. 2023;13(6):1101.
36. Young ML, Schnepp S, Casadio F, Lins A, Meighan M, Lambert JB, et al. Matisse to Picasso: a compositional study of modern bronze sculptures. Anal Bioanal Chem. 2009;395:171–84.
37. Day J, Stenger J, Eremin K, Khandekar N, Budny V. Gaston Lachaise's bronze sculpture in the Fogg Museum. JAIC. 2010;49:1–26.
38. Ganio M, Salvant J, Walton M. From sculptures to foundries: elemental analysis to determine the provenance of modern bronzes. In Proceedings of the 15ème journées d'étude de la SFIIC-ICOMOS. 2014;136–144.
39. Young ML, Dunand DC. Comparing compositions of modern cast bronze sculptures: optical emission spectroscopy versus X-ray fluorescence spectroscopy. JOM. 2015;67:1646–58.
40. Randall M, Zycherman L, Griffith R. Conservation of Joan Miró's bronze sculptures at the Museum of Modern Art. AIC Obj Specialty Group Postprints. 2016;23:233–55.
41. Pouyet E, Ganio M, Motlani A, Saboo A, Casadio F, Walton M. Casting light on 20th-century parisian artistic bronze: insights from compositional studies of sculptures using hand-held X-ray fluorescence spectroscopy. Heritage. 2019;2:732–48.
42. Kwon HH. The corrosion characteristics and applicability of non-destructive investigation in the outdoor bronze sculptures [Ph.D. thesis]. Gongju, Korea: Kongju National University; 2023. p. 6–43.
43. National Institute of Environmental Research. Annual report of air quality in Korea 2022. Incheon, Korea: National Institute of Environmental Research. 2023;21-25:61–79
44. Marušić K, Ćurković HO, Takenouti H. Corrosion inhibition of bronze and its patina exposed to acid rain. J Electrochem Soc. 2013;160(8):C356.
45. Arli BD, Franci GS, Kaya S, Arli H, Colomban P. Portable x-ray fluorescence (p-XRF) uncertainty estimation for glazed ceramic analysis: case of iznik tiles. Heritage. 2020;3(4):1302–29.
46. Jeong YB. Development of Cu based color metal alloy with transition energy and intermetallic compound [Masters theses]. Seoul: Sejong University; 2018. p. 71–2.
47. Strandberg H. Perspectives on sculpture conservation : modelling copper and bronze corrosion [Ph.D. thesis]. Gothenburg: University of Gothenburg; 1997. p. 7–107.

Publisher's Note